6-8-2021

Study of quasimonoenergetic electron bunch generation in self-modulated laser wakefield acceleration using TW or sub-TW ultrashort laser pulses

E. P. Maldonado

R. E. Samad

A. Bonatto

R. P. Nunes

S. Banerjee

See next page for additional authors

Authors
E. P. Maldonado, R. E. Samad, A. Bonatto, R. P. Nunes, S. Banerjee, and N. D. Vieira

AIP Advances

Study of quasimonoenergetic electron bunch generation in self-modulated laser wakefield acceleration using TW or sub-TW ultrashort laser pulses

Cite as: AIP Advances **11**, 065116 (2021); https://doi.org/10.1063/5.0052831
Submitted: 01 April 2021 . Accepted: 24 May 2021 . Published Online: 08 June 2021

E. P. Maldonado, R. E. Samad, A. Bonatto, R. P. Nunes, S. Banerjee, and N. D. Vieira

Study of quasimonoenergetic electron bunch generation in self-modulated laser wakefield acceleration using TW or sub-TW ultrashort laser pulses

Cite as: AIP Advances 11, 065116 (2021); doi: 10.1063/5.0052831
Submitted: 1 April 2021 • Accepted: 24 May 2021 •
Published Online: 8 June 2021

E. P. Maldonado,[1,a)] R. E. Samad,[2] A. Bonatto,[3] R. P. Nunes,[4] S. Banerjee,[5,b)] and N. D. Vieira Jr.[2]

AFFILIATIONS

[1] Instituto Tecnológico de Aeronáutica, ITA, São José dos Campos 12228-615, Brazil
[2] Instituto de Pesquisas Energéticas e Nucleares, IPEN-CNEN/SP, São Paulo 05508-000, Brazil
[3] Universidade Federal de Ciências da Saúde de Porto Alegre, UFCSPA, Porto Alegre 3303-8804, Brazil
[4] Universidade Federal do Rio Grande do Sul, UFRGS, Porto Alegre 90040-060, Brazil
[5] University of Nebraska–Lincoln, UNL, Lincoln, Nebraska 68588, USA

[a)] **Author to whom correspondence should be addressed:** puig@ita.br
[b)] **Current address:** Arizona State University (ASU), Tempe, Arizona 85281, USA.

ABSTRACT

This work presents a study on laser wakefield electron acceleration in the self-modulated regime (SM-LWFA) using 50-fs laser pulses with energy on the mJ scale, at $\lambda = 0.8\ \mu$m, impinging on a thin H_2 gas jet. Particle-in-cell simulations were performed using laser peak powers ranging from sub-terawatt to a few terawatts and plasma densities varying from the relativistic self-focusing threshold up to values close to the critical density. The differences in the obtained acceleration processes are discussed. Results show that bunched electron beams with full charge on the nC scale and kinetic energy in the MeV range can be produced and configurations with peak density in the range $0.5–5 \times 10^{20}$ atoms/cm^3 generate electrons with maximum energies. In this range, some simulations generated quasimonoenergetic bunches with ~0.5% of the total accelerated charge and we show that the beam characteristics, process dynamics, and operational parameters are close to those expected for the blowout regime. The configurations that led to quasimonoenergetic bunches from the sub-TW SM-LWFA regime allow the use of laser systems with repetition rates in the kHz range, which can be beneficial for practical applications.

I. INTRODUCTION

While in conventional electron accelerators the energy gain is based on resonant radio frequency (RF) cavities,[1] a new generation of accelerators uses plasmas to produce strong driving electric fields.[2,3] Superconducting RF cavities reach and can exceed 100 MV/m, but plasma-based systems[4] provide accelerating fields up to TV/m. In the latter, a perturbation is introduced in the plasma to cause local electron displacements, generating non-equilibrium local electric fields, which, in turn, oscillate at the plasma frequency. As the source of perturbation travels along the medium, the local fields also propagate with it and a so-called plasma wakefield is formed. The perturbation can be induced by a charged particle beam, as in plasma wakefield accelerators (PWFAs), or by a laser pulse, as in laser wakefield accelerators (LWFAs). In the latter, the oscillating transverse field of the laser pulse is converted by the plasma into a longitudinal accelerating field with an amplitude that scales with the square root of the plasma density. The high accelerating gradients in these systems allow the production of high-energy bunched electron beams, up to GeV, in compact systems.[5] Many facilities worldwide continue to explore the frontiers for producing even stronger wakefields to reach 10 GeV electrons and beyond.[6,7]

In addition, increasing the repetition rate of the accelerated beams to the kHz scale is a real need for many applications, such as those in which scanning and/or data collection statistics are required.[8,9] The development of high repetition rate laser wakefield electron accelerators also aims its use for ultrafast imaging, matter probing, and isotope production.[4,10,11] In Refs. 12, 13, and 14, a laser spectral broadening technique has been reported, producing laser pulses of 3.5 fs at 1 kHz, with a peak power of 0.8 TW. With such advances in laser technology, adequate excitation at the kHz repetition rate can now be achieved and, in association with plasmas with the appropriate density profile, operated in the so-called *blowout* LWFA regime.[15,16]

On the other hand, tabletop ultrashort laser sources using only a few (1–2) stages of chirped pulse amplification (CPA), such as Ti:sapphire and Yb:glass systems, provide hundreds of GW pulses at kHz or TW pulses at tens of Hz, with longer pulse durations around 100 fs.[17,18] Since these high-peak-power tabletop systems are widely available today and are easier to operate, many facilities are focused on using these conventional laser sources to achieve ~kHz repetition rates in laser electron acceleration.[19,20] Among the LWFA regimes, the SM-LWFA[21,22] has features suitable for operation with these conventional tabletop sources. In this regime, the laser self-focusing effect produces a near diffraction limited spot, enhancing nonlinearities that cause the self-modulation phenomenon, leading to laser-plasma resonant interaction. When the self-focusing phenomenon balances the diffraction for several plasma periods, acceleration of a multi-MeV bunched electron beam can be obtained. These accelerated electron beams have a broader energy spectrum and greater divergence compared to the *blowout* regime.[5,20]

Both techniques, operating on TW and sub-TW peak laser powers, require plasma targets with high densities, around a tenth of the critical value. Gas jets with a thickness of a few hundred micrometers are used, with either continuous flow[15] or driven by fast valves, enabling up to kHz operation. Using pure H_2, the optical field-induced ionization fully saturates for intensities as low as 10^{14} W/cm^2.[20,23] In these free flow targets, usually with the Mach number from 1 to 6, the necessary densities require backing pressure in the range of 10–1000 bars[24,25] and, in some cases, cryogenic cooling.[26]

Low divergence, quasimonoenergetic electron bunches are generated for particular SM-LWFA configurations as a minor part of the main beam. Despite being a phenomenon demonstrated since 2006,[27,28] which occurs with the critical control of the plasma density, the dynamics of this generation has not yet been widely studied. In Ref. 29, quasimonoenergetic electron bunches were generated by SM-LWFA in a process using 9 TW laser pulses and a tenuous He gas target with a thickness of ~1 mm. This generation was associated with the experimental observation that the regime has evolved to operate in the *blowout* mode, tr iggered by the self-modulated laser pulse. In Ref. 30, similar bunches were obtained in a setup with even more tenuous He gas targets and 8 TW laser pulses, in a regime not fully identified. The first realization of SM-LWFA with sub-TW laser pulses (although sub-TW SM-LWFA has been tested before[31]) used much denser and shorter H_2 gas flow targets of 150–250 μm FWHM.[32] In that work, quasimonoenergetic electron bunches were observed to occur at specific plasma densities and peak laser powers, but no study has been reported so far to correlate these results with a *blowout* mode. All these demonstrations used lasers operating at $\lambda \approx 0.8$ μm or $\lambda \approx 1$ μm,[31,33] but SM-LWFA with laser pulses of ~200 GW at $\lambda \approx 4$ μm has also been reported,[34] with characteristics and electron beams analogous to those obtained in Ref. 32, likewise reporting the generation of quasimonoenergetic electron bunches.

In this work, we simulate the SM-LWFA regime using typical ultrashort laser pulses from the conventional tabletop sources mentioned. The simulated target was formed by a jet of H_2 gas with an extension of 120 μm FWHM, whose laser-induced ionization was also calculated during the laser pulse propagation. We choose the laser parameters we have in our laboratory, the same ones used in some reference works:[30,32] $\lambda \approx 0.8$ μm and incident pulse duration of 50 fs, considering laser peak powers from 0.25 to 4 TW. For each of these parameters, we also examine the range of possible plasma densities whose lower limit provides relativistic laser self-focusing and the upper limit is 80% of the critical plasma density. In all studied configurations, the initial (incident) laser pulse is not resonant with the plasma target and self-modulated wakefield acceleration occurs. The charge, energy, and emittance of the resulting accelerated electrons were quantified, allowing a direct comparison of the beams obtained for each process. For some configurations, the generation of quasimonoenergetic bunches occurred as part of the results. These bunches are the main object of this study, and their characteristics and possible mechanisms of generation were investigated.

II. LWFA, DLA, and SM-LWFA

A laser pulse with angular frequency ω and initial duration τ_0 impinges on an *underdense* plasma, with the electron density, n_e, below the critical electron density, $n_e < \epsilon_0 m_e(\omega/e)^2 \equiv n_{cr}$, where ϵ_0 is the vacuum permittivity, m_e is the relativistic electron mass, and e is the elementary charge. The *plasma frequency*, $\omega_p = (e/\epsilon_0{}^{1/2}) \times (n_e/m_e)^{1/2}$, defines the laser phase velocity $v_p = c/[1 - (\omega_p/\omega)^2]^{1/2}$ and group velocity $v_g = c \times [1 - (\omega_p/\omega)^2]^{1/2}$, where c is the speed of light in vacuum. The laser pulse generates ponderomotive forces that excite oscillations at ω_p so that its propagation is followed by a plasma wake with wavelength $\lambda_p \approx 2\pi c/\omega_p$. When the *dimensionless laser amplitude*, a_0, is above unity, $a_0 \equiv eE_0/(\omega m_e c) > 1$, where E_0 is the laser electric field peak amplitude, this wakefield starts to present ion cavities with a sawtooth-like longitudinal electric field.[5] Background electrons can be trapped in the ion cavities after a wave break,[5,35] for instance, and then accelerated.

A. Blowout LWFA and SM-LWFA regimes

If the plasma density is adjusted such that $c\tau_0 \lesssim \lambda_p/2$ and the laser beam diameter is around λ_p, a wakefield with near spherical cavities can be generated.[5] This allows operation in the *blowout* regime,[14] thus generating quasimonoenergetic electrons as long as the laser meets the usual criterion that its peak power, P_L, exceeds the critical power, $P_c^{(b)}$, where[36]

$$P_c^{(b)}[\mathrm{GW}] = 30(\tau_0[\mathrm{fs}]/\lambda[\mu\mathrm{m}])^2. \quad (1)$$

Since this is not attainable when using the conventional tabletop laser systems mentioned above, an alternative is to operate in

the *self-modulated laser wakefield acceleration* (SM-LWFA) regime, conceived in the early 1990s,[21,28,37] as long as the plasma density is now readjusted so that the peak laser power exceeds the *critical power for self-focusing*,

$$P_c[\mathrm{GW}] = 17(n_{cr}/n_e). \quad (2)$$

In this case, the laser pulse can be modulated by the heterogeneous distribution of plasma density, evolving into a fragmented envelope, and these pulse fragments are now resonant with the wakefield. Thin targets are typically used due to the short dephasing length, L_d, given by $L_d = \lambda_P^3/2\lambda^2$, and to a limited extent that the self-focusing phenomenon balances the diffraction (few Rayleigh lengths).[5,20,32,34]

B. Direct laser acceleration

Trapped electrons perform oscillations at the *betatron* frequency, $\omega_\beta = \omega_p/(2\gamma_e)^{1/2}$, where $\gamma_e = (1 + u_x^2 + u_y^2 + u_z^2)^{1/2}$ is the electron relativistic factor and u_x, u_y, u_z are its linear momenta in each direction, in units of m_0c (m_0 is the electron rest mass).[38] The electron acceleration can also be driven by the resonant interaction between these oscillations and the laser magnetic field. This phenomenon is called *direct laser acceleration* (DLA)[39,40] and depends on the pulse-wake superposition parameter $T_p = c\tau_L/\Lambda_{wake}$, where τ_L is the laser pulse (or fragment) duration and $\Lambda_{wake} = (a_0)^{1/2}\lambda_p$ is the nonlinear wavelength.[41,42]

The frequency of the laser in the electron frame is Doppler shifted, $\omega_D = \omega[1 - (u_z c)/(\gamma_e v_p)]$, and DLA requires that it must correspond to a harmonic of ω_β,[43]

$$N = \omega_D/\omega_\beta = 1,\ 2,\ 3,\ \ldots, \quad (3)$$

which occurs only in some parts of the acceleration path.[32,43,44] In SM-LWFA, DLA can occur and be a relevant additional acceleration mechanism.[32,45]

C. SM-LWFA and regions of operation

There are three distinct operating ranges (or sub-regimes) for SM-LWFA.[34] Referring to the self-focusing collapse position, z', the first range of parameters leads to z' occurring in a low-density region. The laser beam undergoes moderate self-focusing and moderate self-modulation, resulting in little electron entrapment and a low-charge electron beam. In the second range of parameters, z' occurs in a region with enough density, leading to a strong self-modulation, followed by self-channeling, and a beam of electrons with a higher charge and energy is produced.[5,31] The third region of parameters is associated with denser, near critical plasmas, presenting shorter dephasing lengths and a beam of accelerated electrons with a lower quality than in the previous cases.[46]

III. RESEARCH METHOD

Our simulations were performed using the quasi-cylindrical (quasi-3D), Fourier–Bessel Particle-In-Cell (FBPIC) code originally developed by Remi Lehe at Lawrence Berkeley National Laboratory and Manuel Kirchen at CFEL, Hamburg University.[47] The local density of plasma electrons is calculated from the neutral gas using the Ammosov–Delone–Krainov (ADK) ionization model.[48] In the simulations, the volume evaluated at each step has radius $R = 20\ \mu$m and length $\Delta z = 100\ \mu$m. The spectral calculation is performed considering three azimuthal modes. Fields are evaluated in a grid that has 3750 points in Δz and 600 points in R, a density that corresponds to 30 points/λ, in the longitudinal direction, and 30 points/w_{min}, in the radial direction (estimating an approximate value for the minimum laser beam waist $w_{min} \approx 1\ \mu$m), a resolution similar to that used in Ref. 49, for example. The number of particles per cell (ppc) is 2 along z, 2 along r, and 12 along θ, following the developer recommendation.[50]

In this study, the targets were considered as cylindrical H_2 gas jets flowing in the y direction and with a diameter of 200 μm. The laser pulse propagates in the z direction and passes through the target center. The gas density has a radial symmetrical profile with a linear ascending ramp of 80 μm and a central plateau, therefore a trapezoidal profile with 120 μm FWHM, in a diametrical cut (see Fig. 1). This is a good representation for the flow from a submillimetric supersonic nozzle.[51,52] The background is assumed to be absolute vacuum.

There is only one ionization per atom, so the plasma density, n_e, is the same as the hydrogen atom density, n_{atoms}, for saturated ionization. We define the plateau plasma density as $n_{e,0}$. An example of this distribution cross section (along the z axis) for $n_{e,0} = 2 \times 10^{20}$ cm^{-3} is shown in Fig. 1, as well as the calculated local plasma wavelength.

The main laser and plasma parameters used in the simulations are given in Table I. Here, some parameter values are the simulation input (defining the physical system) and others are calculated and presented to facilitate the analysis. The relevant computing parameters are given in Table II.

The laser pulse is linearly polarized in the x direction and starts at $z = -50\ \mu$m. In all configurations, the laser power is above the critical power for self-focusing (expression 2, using $n_{e,0}$ as n_e). The laser beam, assumed ideal Gaussian with $M^2 = 1$, is focused on vacuum (without the target) at $z = 40\ \mu$m to $w_0 = 7\ \mu$m (this w_0 is ~9λ, similar to those in Refs. 20, 32 and 34).

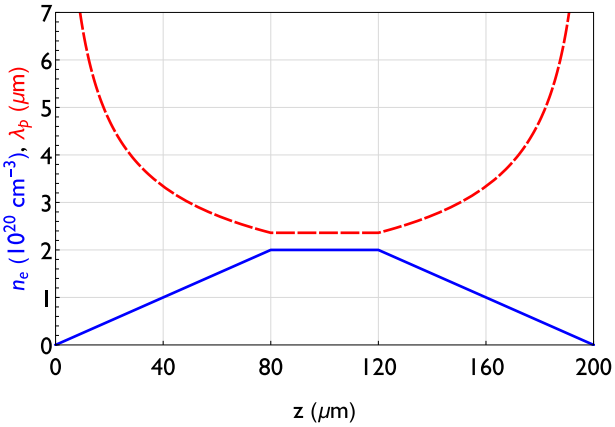

FIG. 1. Blue curve (continuous line): distribution of electron density after ionization, $n_e(z)$, equivalent to the atomic density for the H_2 gas jet with 2×10^{20} cm^{-3} peak. Red curve (dashed line): calculated, local nominal plasma wavelength (without local relativistic or density variation effects).

TABLE I. Laser and plasma parameters used in the simulations. Asterisk values are the independent input data. MIV: measured in vacuum. Values of I_0 and a_0 are at the vacuum propagating beam focus position.

Physical parameter	Value
Laser, initial pulse duration (FWHM), τ_0 (fs)	50
Laser, initial peak power, P_L (TW)	$1/4$, $1/2$, 1, 2, 4
* Laser, wavelength, λ (μm)	0.8
* Laser, pulse center start position, z_0 (μm)	−50
* Laser (MIV), pulse length (FWHM), $L_0 = c\tau_0$ (μm)	15
* Laser (MIV), focus position, z_{foc} (μm)	40
* Laser (MIV), beam waist, w_0 (μm)	7.0
* Laser (MIV), incident amplitude, a_0	0.4–1.6
Laser (MIV), Rayleigh range, z_R (μm)	192
Laser (MIV), intensity, I_0 (10^{17} W cm^{-2})	3–50
* Target, species (gas)	H^2
* Target, top atomic density, n_{atoms} (10^{19} cm^{-3})	1–140
* Target, start position in z (μm)	0
* Target, total z-extension (μm)	200
* Target, length of entry and exit ramps (μm)	80
Plasma, wavelength, λ_p (μm)	1–10.5
Plasma, dephasing length, L_d (μm)	1–912
Plasma, group velocity (v_g/c)	0.44–1

TABLE II. Computing parameters in simulations. The number of particles per cell is 2 along z, 2 along r, and 12 along θ.

Simulation parameter	Value
Start position of the simulation box (μm)	−100
Simulation box length, Δz (μm)	100
Simulation box diameter, $2R$ (μm)	40
Number of grid points along z	3750
Number of grid points along r	600
Number of azimuthal modes, n_m	3
Number of particles per cell	48
Speed of the moving window, $v_w(c)$	0.6–1
Simulation time step, Δt (as)	89
Simulation length, maximum z (μm)	~300

The general configuration is similar to that found in the first SM-LWFA experiments using sub-TW laser pulses.[20,32] Since the considered plasma densities range from $n_{e,0}/n_{cr} \approx 0.006$ to $n_{e,0}/n_{cr} \approx 0.8$ and the electrons can be subjected to deceleration from dephasing, we have chosen to save and analyze electrons with $u_z \geq 0.1\ m_0c$, which is equivalent to energies above ~2.5 keV. Electrons of all energies are considered when running the simulations.

IV. RESULTS

A. Ranges of acceleration processes

In this section, we describe the parameter ranges for SM-LWFA that led to similar behaviors in processes and results, as stated in Sec. II. In the *first parameter range*, self-focusing and self-modulation occurred with maxima in a position (z') around the middle of the density exit ramp. The acceleration processes had the following characteristics:

- a nonlinear wakefield was excited when the laser pulse approached z';
- extensive self-channeling did not occur;
- laser pulse fragments, after self-modulation, presented a superposition parameter of $0.8 \leq T_p < 2$;
- the generated electron beam was composed by bunches with duration in the range of fs to tens of fs and low divergence;
- no quasimonoenergetic bunch was obtained; and
- under the same initial laser peak power, the maximum electron energy increases with the plasma density.

In our study, the results with characteristics in this range occurred for the following configurations:

- $P_L = 1/4$ TW, $n_{e,0} < 5 \times 10^{20}$ cm^{-3};
- $P_L = 1/2$ TW, $n_{e,0} < 2 \times 10^{20}$ cm^{-3};
- $P_L = 1$ TW, $n_{e,0} < 1 \times 10^{20}$ cm^{-3};
- $P_L = 2$ TW, $n_{e,0} < 5 \times 10^{19}$ cm^{-3}; and
- $P_L = 4$ TW, $n_{e,0} < 3 \times 10^{19}$ cm^{-3}.

As an example, we highlight the simulation using incident peak power $P_L = 1$ TW, $a_0 \approx 0.8$, and target peak density $n_{e,0} = 7 \times 10^{19}$ cm^{-3} (~0.04 n_{cr}). The maximum field and minimum duration occur at $z' \approx 164$ μm, with a new laser amplitude $a_0' \approx 1.7$ and a main fragment length $L_0' \approx 5.9$ μm. A nonlinear wakefield is formed, persisting until the end of the target. When comparing L_0' with the simulated nonlinear plasma wavelength, the superposition parameter found is $T_p \approx 1.2$.

The transverse momentum angles, right after the electrons leave the target, $x' = u_x/u_z$ and $y' = u_y/u_z$, were determined as functions of x and y, respectively. The normalized transverse *rms* emittance in the x direction, $\varepsilon_{x,rms} = [\langle x^2\rangle\langle y_e{}^2(x')^2\rangle - \langle xy_ex'\rangle^2]^{1/2}$, was then calculated, resulting in $\varepsilon_{x,rms} \approx 7.5$ mm mrad. An analogous formula applies to the y direction,[53] and we obtained $\varepsilon_{y,rms} \approx 8.0$ mm mrad. The energy spectrum of the electrons is quasi-exponential, presenting a median value of 0.34 MeV and a maximum of 9 MeV. The nominal dephasing length (at the plateau) is longer than 50 μm (a typical value for this range of SM-LWFA); thus, this acceleration process could be performed in slightly thicker targets.

The *second parameter range* led to self-focusing and self-modulation with maxima near the end of the density plateau. A nonlinear wakefield was excited, and the acceleration processes had the following characteristics:

- subsequent laser self-channeling occurred;
- laser pulse fragments presented a superposition parameter of $0.3 \leq T_p < 1$;
- the generated electron beam was composed by bunches with duration in the range of a few fs and moderate divergence;
- quasimonoenergetic bunches occurred; and
- under the same initial laser peak power, the maximum electron energy does not change significantly with plasma density.

The simulation results that shared these similarities occurred for the following configurations:

- $P_L = 1/2$ TW, $n_{e,0} \in [2, 3] \times 10^{20}$ cm^{-3};
- $P_L = 1$ TW, $n_{e,0} \in [1, 3] \times 10^{20}$ cm^{-3};
- $P_L = 2$ TW, $n_{e,0} \in [0.5, 3] \times 10^{20}$ cm^{-3}; and
- $P_L = 4$ TW, $n_{e,0} \in [0.3, 2] \times 10^{20}$ cm^{-3}.

As representative of these processes, we highlight the configuration using $P_L = 1/2$ TW, $a_0 \approx 0.6$, and peak density $n_{e,0} = 2 \times 10^{20}$ cm^{-3} ($\sim 0.1\ n_{cr}$). The laser pulse has the maximum field and minimum duration at $z' \approx 140\ \mu$m, with a new laser amplitude $a_0' \approx 1.4$ and a main fragment length $L_0' \approx 1\ \mu$m. A nonlinear wakefield is formed, persisting until the end of the target, and the superposition parameter is $T_p \approx 0.3$.

Trapped electrons are accelerated along an extension that corresponds to most of the downramp (although the nominal dephasing length is only $L_d \approx 10\ \mu$m on the target plateau). Figures 2(a) and 2(b) show two x–z cross sections of the charge density field: (a) the nonlinear wakefield in the middle of the downramp and (b) the electrons leaving the target. The bunch on the right in Fig. 2(b), highlighted by the dashed rectangle, is quasimonoenergetic, with a mean energy of 8.4 MeV and FWHM of 2.6 MeV, while the remaining

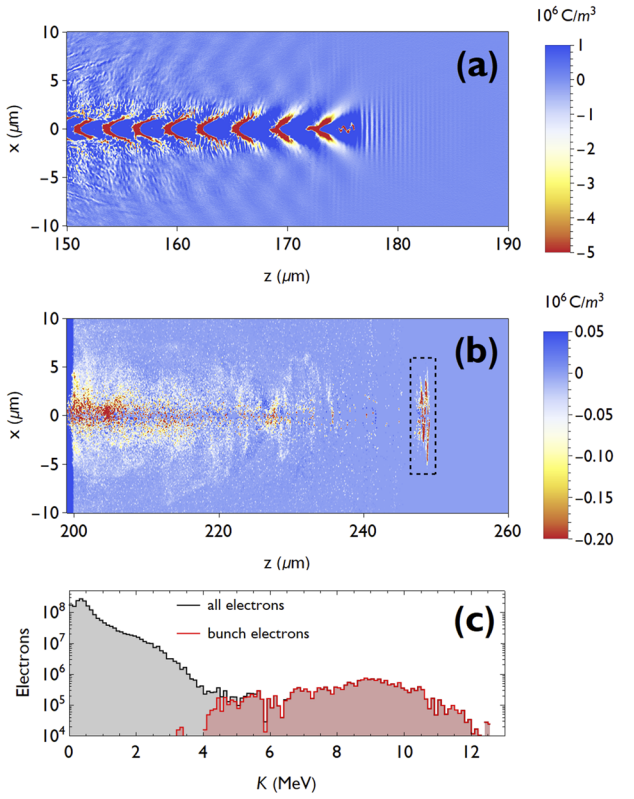

FIG. 2. In (a) and (b), snapshots of the charge density field in the x–z plane, $\rho(x, z)$, from the simulation with initial $P_L = 1/2$ TW and target peak electron density $n_{e,0} = 2 \times 10^{20}$ cm^{-3}. The color scales are saturated, and the full-scale values are $[-9.2, 2.2] \times 10^7$ C/m^3 in (a) and $[-7.9, 3.1] \times 10^6$ C/m^3 in (b). Part (c) presents the energy distribution of all electrons leaving the target in a histogram with 120 bins over the entire energy range. The highlighted portion of the spectrum (in red) corresponds to that of the highlighted quasimonoenergetic bunch [dashed rectangle in (b)].

electrons show a quasi-exponential distribution with a median of 0.4 MeV, as shown in the energy spectrum in Fig. 2(c).

The transverse normalized *rms* emittances of the accelerated beam were calculated just as before. Considering all the electrons leaving the target, $\varepsilon_{x,rms} \approx 11.5$ mm mrad and $\varepsilon_{y,rms} \approx 9.8$ mm mrad. The quasimonoenergetic bunch has much lower values: $\varepsilon_{x,rms} \approx 0.6$ mm mrad and $\varepsilon_{y,rms} \approx 0.3$ mm mrad.

In the *third parameter range*, self-focusing and self-modulation presented maxima in the first half of the target. Processes had the following characteristics:

- the laser beam faded quickly, permanently diffracted right after z'; laser self-channeling did not occur;
- other weaker local maxima sometimes occur; nonlinear wakefields are formed close to the positions of the maximum laser amplitude;
- the laser pulse fragments presented a superposition parameter $T_p \lesssim 1$;
- the electron beam has a duration of several tens of fs, with lower energy and a broad, quasi-exponential spectrum;
- no quasimonoenergetic bunch is obtained; and
- under the same initial laser peak power, the maximum electron energy decreases with increasing plasma densities.

In our study, these occurred for the following configurations:

- $P_L = 1/4$ TW, $n_{e,0} \gtrsim 5 \times 10^{20}$ cm^{-3};
- $P_L = 1/2$ TW, $n_{e,0} > 3 \times 10^{20}$ cm^{-3};
- $P_L = 1$ TW, $n_{e,0} > 3 \times 10^{20}$ cm^{-3};
- $P_L = 2$ TW, $n_{e,0} > 3 \times 10^{20}$ cm^{-3}; and
- $P_L = 4$ TW, $n_{e,0} > 2 \times 10^{20}$ cm^{-3}.

Here, we highlight the simulation with incident peak power $P_L = 1$ TW, $a_0 \approx 0.8$, and target peak density $n_{e,0} = 6.3 \times 10^{20}$ cm^{-3} ($\sim 0.4\ n_{cr}$). The laser pulse shows a maximum amplitude $a_0' \approx 2.3$ at $z' \approx 76\ \mu$m. The main fragment has $L_0' \approx 0.9\ \mu$m, and the superposition parameter at z' is $T_p \approx 0.5$. The electrons leaving the target exhibit a quasi-exponential energy spectrum with 0.51 MeV median and 6 MeV maximum. The obtained normalized *rms* emittances of the accelerated beam are $\varepsilon_{x,rms} \approx 13.9$ mm mrad and $\varepsilon_{y,rms} \approx 15.1$ mm mrad.

B. Comparative study

Figure 3 presents the energy distributions of the electrons that just left the target for $P_L = 1$ TW and cases in each of the three ranges discussed. The processes show spectra that contain Maxwellian-like, quasi-exponential distributions, with median energies of (a) 0.34 MeV, (b) 0.40 MeV, and (c) 0.51 MeV. In case (b), the spectrum also contains a second distribution that corresponds to a quasi-monoenergetic bunch similar to that highlighted on the right in Fig. 2(b), presenting a mean value of 10.6 MeV and a FWHM of 10.4 MeV. The phenomenon "two-temperature distribution" has similar spectral characteristics, frequently attributed to a "population of hot electrons heated directly by the laser"[44] and is also seen in SM-LWFA.[31,54] However, the high-energy part of the spectrum in Fig. 3(b) (in red) was obtained in this case entirely from a distinct ultrashort electron bunch, spatially separated and ahead of the background electrons.

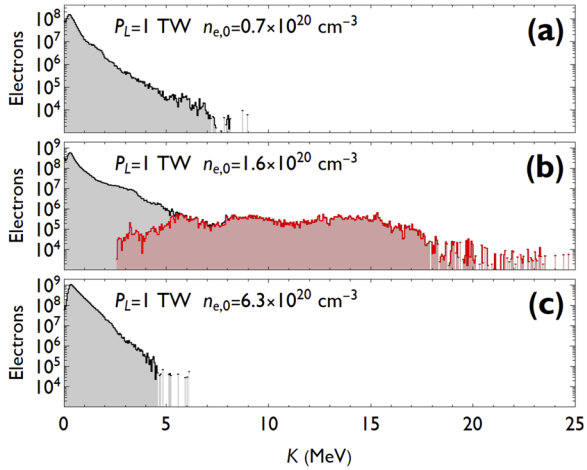

FIG. 3. Energy distributions of the electrons leaving the target from three example simulations with initial P_L = 1.0 TW ($a_0 \approx 0.8$) and peak densities (a) $n_{e,0}$ = 7 × 10^{19} cm^{-3}, (b) $n_{e,0}$ = 1.6 × 10^{20} cm^{-3}, and (c) $n_{e,0}$ = 6.3 × 10^{20} cm^{-3}. The histograms have 500 bins over the entire energy range. In (b), the highlighted portion of the spectrum (in red) corresponds to a quasimonoenergetic bunch.

The results in Figs. 4–7 show the calculated values for the main parameters of all electron beams obtained as a function of the peak plasma density in the target (on the plateau) and the incident laser peak power. The electrons were considered immediately after leaving the target. Figure 4 presents a plot of the total charge, Q_T (absolute value), which, as a general trend, grows with $n_{e,0}$. We defined a reference kinetic energy for the electron beam as its median value, $\tilde{K}$, whose values show a peak around 2 × 10^{20} cm^{-3} (Fig. 5). Another parameter of interest is the maximum kinetic energy of the electrons in the beam, K_{max}, which shows peaks distributed in the range from 5 × 10^{19} to 5 × 10^{20} cm^{-3} with higher density values for decreasing laser power (Fig. 6).

We evaluated the normalized transverse rms emittance for electrons with longitudinal momentum $u_z \geq m_0 c$, thus corresponding to $K \geq 0.21$ MeV, justified by the fact that the studied processes occur using peak plasma densities over a range of two orders of

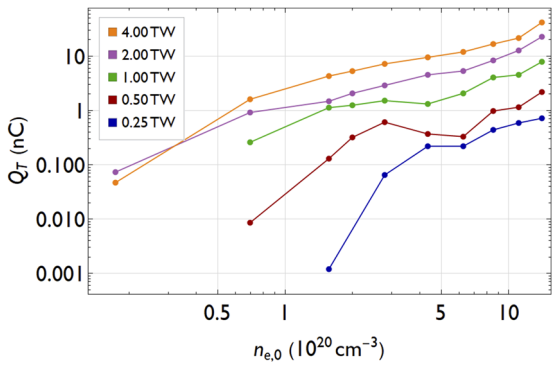

FIG. 4. Total charge of the electrons leaving the target, as a function of the peak plasma density, for all the studied laser peak power values.

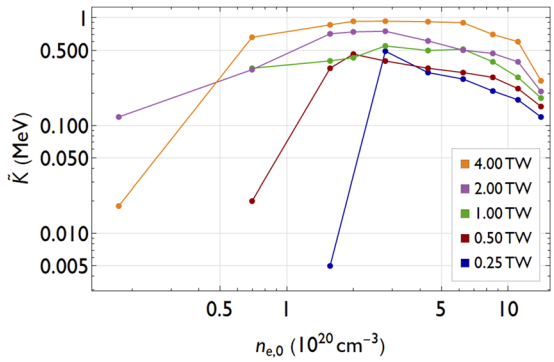

FIG. 5. Reference energy of the electrons leaving the target, as a function of the peak plasma density, for all peak laser powers.

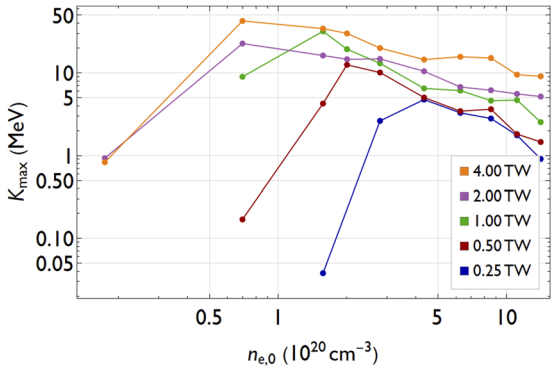

FIG. 6. Maximum energy of the electrons leaving the target, as a function of the peak plasma density, for all peak laser powers.

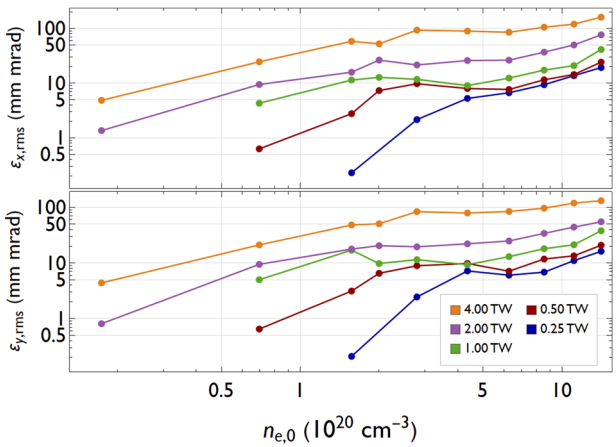

FIG. 7. Normalized transverse *rms* emittances of all electrons leaving the target, in the *x* (upper graph) and *y* (lower graph) directions, as functions of the peak plasma density, for all peak laser powers. Electrons with energy above 0.21 MeV were considered.

TABLE III. Selected configurations generating well-formed quasimonoenergetic bunches obtained at each laser peak power and respective initial parameters P_L and $n_{e,0}$. Also shown are the maximum laser amplitude, a_0', and its average value along the segment of acceleration, $\langle a_0 \rangle$. Q_b is the quasimonoenergetic bunch charge, K_b is its mean energy, ΔK_b is its energy width (FWHM), and $\varepsilon_{x,rms}$, $\varepsilon_{y,rms}$ are its transverse normalized emittances.

P_L (TW)	$n_{e,0}$ (10^{20} cm^{-3})	a_0' $\langle a_0 \rangle$	Q_b (pC)	K_b (MeV)	ΔK_b (MeV)	$\varepsilon_{x,rms}\varepsilon_{y,rms}$ (mm mrad)
0.5	2.0	1.4 1.3	4	8.4	2.6	0.6 0.3
1.0	1.6	2.7 2.3	12	11	10	1.8 5.4
2.0	1.6	4.4 3.5	259	4.6	4.6	7.2 8.3

magnitude. As a result, both transverse normalized emittances show values from few tenths to several tens, increasing with the density of the plasma, as shown in Fig. 7. Note that in the previously cited experimental works,[20,32] the beam emittance is quantified only for electrons with energies above 1 MeV, which leads to lower values.

The well-formed quasimonoenergetic bunches are those spatially and energetically separated (for the most part) from the background electrons, such as the example shown in Figs. 2(b) and 2(c). The parameters of some well-formed quasimonoenergetic bunches obtained for different initial laser peak powers, P_L, are listed in Table III, where Q_b is the bunch charge, K_b is its central energy (mean value), ΔK_b is its energy width (FWHM), and $\varepsilon_{(x,y),rms}$ is the transverse emittance. Also shown are the peak plasma density, $n_{e,0}$; the maximum laser amplitude, a_0'; and its average value in the wakefield $\langle a_0 \rangle$.

V. DISCUSSION AND CONCLUSIONS

A. Quasimonoenergetic bunches

Well-formed bunches were obtained for incident peak laser powers in the range of 0.5–2 TW and for peak densities between 1.5×10^{20} and 2.0×10^{20} cm^{-3}. For parameters slightly outside this range (P_L, $n_{e,0}$), bunches with quasimonoenergetic characteristics are not well formed, spatially or in energy, or do not appear at all. Although in some cases we were limited by the discrete values of the parameters used, this behavior was a consequence of the general configuration parameters (density profile, gas species, and initial focus of the laser beam) chosen close to the experimental realizations of sub-TW SM-LWFA regimes. The emittances $\varepsilon_{(x,y),rms}$ are of the order of a few mm mrad in the first two lines of Table III, but higher values are obtained for P_L = 2 TW ($n_{e,0} = 1.6 \times 10^{20}$ cm^{-3}), which is related to the fact that the best simulated density in this case is not yet ideal (this can also be inferred from the lower value of K_b obtained).

Experimental SM-LWFA studies using sub-TW to few-TW laser pulses have demonstrated[28,32,55] that the quasimonoenergetic bunch charge (Q_b) is typically in the pC range, with fractional charge $Q_b/Q_T \approx 0.2\%$;[32] the central (mean) energy (K_b) is up to 20 MeV; and the width (ΔK_b) is of a few to several MeV. We point that our simulation results are in good agreement with those that occur experimentally.

B. DLA contribution

DLA demands $T_p \gtrsim 0.5$.[32,41] A superposition parameter value $T_p \approx 0.5$ occurred in the processes that gave rise to the beams in Table III. Electron beams generated by DLA-dominated processes have[41] the electric charge accumulating at its transverse ends and the highest-energy electrons presenting the largest divergence. However, in all quasimonoenergetic bunches obtained, no significant charge concentration was found at the transverse ends of the beam and its divergence does not show any significant growth trend with energy.

In addition, where the DLA process is significant, the energy variation of the electrons throughout the acceleration history is synchronized with their betatron oscillations, with energy gain occurring when expression (3) is satisfied. When tracking a macroparticle along the acceleration processes, the energy values can be juxtaposed to its transverse linear momentum in the laser polarization direction and then analyzed. We conducted many of such assessments, and they indicate that the processes in Table III do not have significant acceleration contribution from DLA. This can be seen from the analysis of Fig. 8(a) generated for the configuration $n_{e,0} = 1.6 \times 10^{20}$ cm^{-3}, P_L = 1 TW. This figure shows a graph of the kinetic energy, K, of the 15 highest-energy macroparticles along their acceleration path, as well as their associated transverse momenta, u_x. The highlighted red curve shows the evolution of K for a single macroparticle, and the highlighted blue curve shows its u_x values. The faded colored curves show those quantities for the other macroparticles, evidencing that they have similar evolutions. In this graph, one can see that the energy of the electrons increases smoothly (a monotonic gain), regardless of the transverse momentum oscillations, with some deceleration due to dephasing only near the end of the target.

In turn, the modulation of energy gain in synchronicity with the betatron oscillations can be found among the configurations using P_L = 2 TW or P_L = 4 TW. Figure 8(b) shows an example from the simulation with P_L = 4 TW and $n_{e,0} = 7 \times 10^{19}$ cm^{-3}: a graph of the kinetic energy and the transverse momentum of the 30 highest-energy macroparticles. The transverse momentum, u_x, has periodic values with a length around the calculated betatron wavelength, $\lambda_\beta = \Lambda_{wake}\,(2\gamma_e)^{1/2} \approx 30\ \mu$m, and K changes with $\lambda_\beta/2$, which is a behavior characteristic of the DLA energy gain.[49] Note that in our simulations for P_L = 4 TW, the typical superposition parameter obtained was $T_p \gtrsim 0.8$, therefore exceeding the T_p condition for DLA.

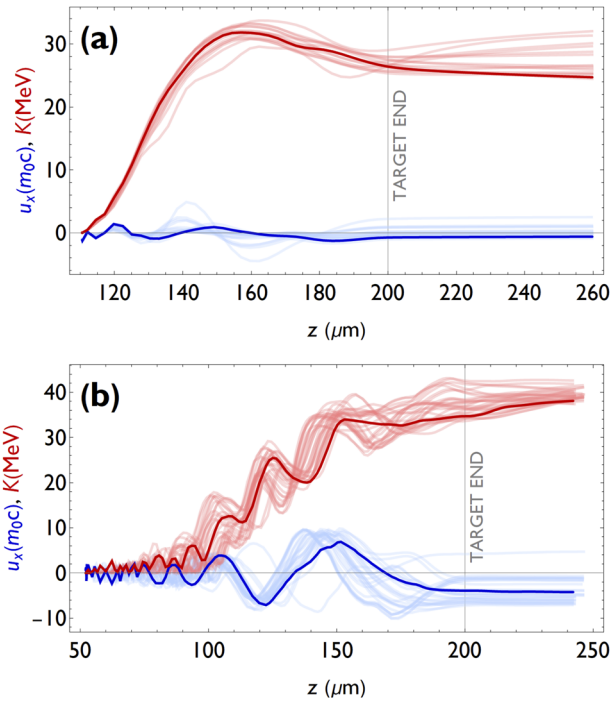

FIG. 8. (a) Kinetic energy (red) and transverse momentum (blue) of (a) the 15 highest-energy macroparticles, throughout the history of their acceleration, in the simulation with P_L = 1 TW and $n_{e,0}$ = 1.6 × 10^{20} cm^{-3} and (b) the 30 highest-energy macroparticles, throughout the history of their acceleration, in the simulation with P_L = 4 TW and $n_{e,0}$ = 7 × 10^{19} cm^{-3}.

C. Blowout regime

As stated in Sec. IV A, in the description of the "*second parameter range*," in the cases that generate quasimonoenergetic bunches, the acceleration processes have the following dynamics. Self-channeled laser propagation occurs, as well as a nonlinear wakefield, along the entire length of the exit ramp. This wakefield is formed by prominent regions of clean positive charge, or ion cavities, albeit with an elongated shape (as can be seen from the typical example in Fig. 2). A small bunch of electrons is trapped in the first and/or second periods of the wakefield, starting from the z' position. The typical energy gain follows the example in Fig. 8(a).

In the simulated configurations presenting quasimonoenergetic bunches, the average superposition parameter at z' is $T_p^{(1)}$ ≈ 0.6, not varying much along the acceleration path (the exit downramp) and the average transverse superposition ratio is w_0'/Λ_{wake} ≈ 0.6. For all simulation results, we obtained the $P_L'/P_c^{(b)}$ ratio, where P_L' is the peak power of the laser pulse fragment at z' and $P_c^{(b)}$ is the *blowout* threshold power, calculated from expression (1) using the parameters of the self-modulated laser pulse, i.e., the fragment duration τ' instead of τ_0. The obtained values are represented by the surface in Fig. 9. It can be easily seen that this ratio is well below the unit (reference plane) in most of the simulations, including those with well-formed quasimonoenergetic bunches, indicated by red dots superimposed on the surface.

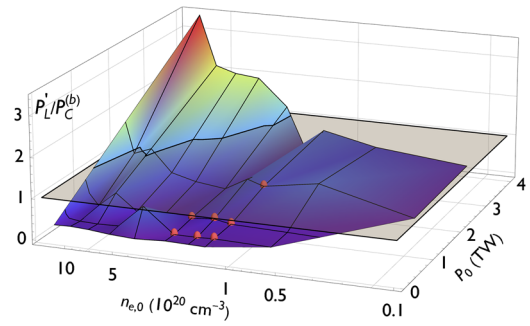

FIG. 9. Ratio of the laser pulse fragment peak power to the calculated critical power for the blowout regime (expression 1), $P_L'/P_c^{(b)}$, for all the studied configurations. The plane $P_L'/P_c^{(b)}$ = 1 is also shown. Red dots: all simulated configurations that show well-formed quasimonoenergetic bunches.

However, it should be noted that expression (1) is derived from a study developed in a specific domain.[36] By defining the similarity parameter $S \equiv n_e/(a_0' n_{cr})$, the source model of expression (1) assumes $S \ll 1$ and $a_0' \gg 1$ (or an *ultra-relativistic, tenuous underdense plasma regime*). Our simulations exhibit quasimonoenergetic electrons from regimes with a_0' of few units and S of several hundreds; therefore, it is useful to compare our results with the predictions of another model, with a more appropriate domain. This is the case of the analytical-heuristic model developed by Lu *et al.*,[56,57] considering the *blowout* LWFA in the case of laser beam channeling. In addition to a condition for the ideal laser spot radius, $w_0/\Lambda_{wake} \approx \pi^{-1}$, and a condition for the laser pulse length, $L_0 \lesssim w_0$, it presents (as its main parameter) the critical laser amplitude $a_{0c} \approx 2\,(n_{cr}/n_e)^{1/2}$. Therefore, this model indicates that smaller values of laser amplitude are needed as the plasma density increases.

Throughout our study, only those simulations that simultaneously exhibited laser self-channeling and focused laser amplitude $a_0' \gtrsim 1.5$ and for which both geometric conditions (transversal and longitudinal) are approximately met produced well-formed quasimonoenergetic bunches. Conversely, bunches with much less distinction (from the accelerated background) were obtained for configurations with $T_p \gtrsim 0.8$ (mainly those using P_L = 4 TW) as well as for those presenting $a_0' \lesssim 1.5$ (mainly those with P_L = 0.25 TW). Finally, we note that it is known from experimental results that the blowout regime can occur even when the laser amplitude is slightly below the a_{0c} threshold and with geometric conditions not strictly fulfilled.[57]

D. Quasimonoenergetic beam applications

Systems designed to operate in the LWFA pure *blowout* regime, at ~kHz repetition rate, use few-cycle laser pulses, with $\tau_0 \leq 5$ fs (at $\lambda \approx 0.8$ μm) and mJ energy. State-of-the-art results in such cases usually generate a beam of quasimonoenergetic bunches with $K_b \approx 5$ MeV, $\Delta K_b/K_b \approx 0.5$, $Q_b \approx 4$ pC, and $\varepsilon_{(x,y),rms} \approx 0.6$ mm mrad, with low dependence on plasma density adjustment.[12,14,58] However, such bunches are often followed by a low-energy background with a much higher normalized transverse emittance (of few orders of magnitude) and comparable charge.[8,16] A noticeable difference between this behavior and the quasimonoenergetic results in TW and sub-TW SM-LWFA is that, in the latter (our case), the

background electrons in the beam have a charge two orders of magnitude greater than that of the quasimonoenergetic bunch. Nevertheless, it should be noted that the quasimonoenergetic parameters have similar values in the two techniques: the mean energy, the energy width (FWHM), the bunch charge, and the transverse emittances. Electron beams with this set of parameters, at a high repetition rate, are suitable for applications such as for ultrafast electron diffraction and pulsed radiolysis. These sources have also been pointed for the irradiation of biological samples, ultrafast imaging, and femtosecond x-ray generation.[14,59]

E. Full beam applications

As is well known, the full beam of accelerated electrons obtained from SM-LWFA has a quasi-exponential spectrum. In our study, most of the charge is in the range of 1 MeV, with transverse emittances of tens of mm mrad ($\lesssim$10 mm mrad for 1 TW and sub-TW). However, the fact that the total charge is on the nC scale makes these beams relevant for applications where a high dose of radiation is required,[46,54,59] with the advantage of allowing compact high repetition rate systems.

F. Summary and conclusions

In this work, we used PIC simulations to study SM-LWFA generated by 50-fs laser pulses at $\lambda = 0.8$ μm with peak powers from 0.25 to 4 TW using a target formed by a jet of H_2 gas with a thickness of 120 μm FWHM. These and the other parameters considered place the simulated configurations close to those of important recent experimental demonstrations.[20,32] The various characteristics of the processes obtained were discussed and classified into three sub-regimes that depend on the initial laser and plasma parameters. In the best cases, laser self-channeling is achieved and a continuous wakefield occurs along the entire exit ramp. These cases are obtained for peak density in the range from 5×10^{19} to 5×10^{20} cm^{-3}, generating electron bunches with total charge on the nC scale. For initial laser peak power in the interval 0.5 to 2 TW and optimal peak plasma density around 2×10^{20} cm^{-3}, well-formed quasimonoenergetic bunches are produced, with central (mean) energy in the range of 5–11 MeV, widths from 3 to 10 MeV (FWHM), about 0.5% of the total charge, and normalized transverse emittances of a few mm mrad. These values are fully in line with the experimental results of TW and sub-TW SM-LWFA. We point out that these quasimonoenergetic bunches can be suitable for many high repetition applications, although further studies on directional and long-term stability are still needed.[59,60] We have also shown that the processes that give rise to such bunches in TW and sub-TW SM-LWFA do not have the typical DLA energy gain, nor the expected DLA signatures are verified on their electrons.[41] Instead, the bunch characteristics and the acceleration history are compatible with those of the *blowout* LWFA. We verified that the configurations that present well-formed quasimonoenergetic bunches have the operational parameters closest, among all tested, to the conditions expected for this regime, considering the theoretical model that assumes laser channeling and no restrictions on plasma density.[57]

ACKNOWLEDGMENTS

We would like to acknowledge the Laboratory for Scientific Computing (LNCC), in Petrópolis-RJ, Brazil, for allowing us to use of the Santos Dumont supercomputer. We also acknowledge the São Paulo Research Foundation (FAPESP) for the funding granted through the Program "São Paulo Researchers in International Collaboration" (SPRINT), Process No. 2018/25961-7.

DATA AVAILABILITY

The data that support the findings of this study are available from the corresponding author upon reasonable request.

REFERENCES

[1] T. P. Wangler, *RF Linear Accelerators* (Wiley, 2008).
[2] T. Tajima and J. M. Dawson, Phys. Rev. Lett. **43**, 267 (1979).
[3] P. Sprangle, E. Esarey, and A. Ting, Phys. Rev. Lett. **64**, 2011 (1990).
[4] B. Hidding, S. Hooker, S. Jamison, B. Muratori, C. Murphy, Z. Najmudin, R. Pattathil, G. Sarri, M. Streeter, C. Welsch, M. Wing, and G. Xia, Plasma wakefield accelerator research 2019–2040: A community-driven UK roadmap compiled by the Plasma Wakefield Accelerator Steering Committee (PWASC), 2019.
[5] E. Esarey, C. B. Schroeder, and W. P. Leemans, Rev. Mod. Phys. **81**, 1229 (2009).
[6] W. P. Leemans, A. J. Gonsalves, H.-S. Mao, K. Nakamura, C. Benedetti, C. B. Schroeder, C. Tóth, J. Daniels, D. E. Mittelberger, S. S. Bulanov, J.-L. Vay, C. G. R. Geddes, and E. Esarey, Phys. Rev. Lett. **113**, 245002 (2014).
[7] A. J. Gonsalves, K. Nakamura, J. Daniels, C. Benedetti, C. Pieronek, T. C. H. De Raadt, S. Steinke, J. H. Bin, S. S. Bulanov, J. Van Tilborg, C. G. R. Geddes, C. B. Schroeder, C. Tóth, E. Esarey, K. Swanson, L. Fan-Chiang, G. Bagdasarov, N. Bobrova, V. Gasilov, G. Korn, P. Sasorov, and W. P. Leemans, Phys. Rev. Lett. **122**, 084801 (2019).
[8] R. Polanek, N. A. M. Hafz, Z. Lécz, D. Papp, C. Kamperidis, S. Brunner, E. R. Szabó, T. Tékés, and K. Hideghéty, Nucl. Instrum. Methods Phys. Res., Sect. A **987**, 164841 (2021).
[9] J. Faure, B. van der Geer, B. Beaurepaire, G. Gallé, A. Vernier, and A. Lifschitz, Phys. Rev. Accel. Beams **19**, 021302 (2016).
[10] Z.-H. He, B. Beaurepaire, J. A. Nees, G. Gallé, S. A. Scott, J. R. S. Pérez, M. G. Lagally, K. Krushelnick, A. G. R. Thomas, and J. Faure, Sci. Rep. **6**, 36224 (2016).
[11] F. Albert and A. G. R. Thomas, Plasma Phys. Controlled Fusion **58**, 103001 (2016).
[12] D. Guénot, D. Gustas, A. Vernier, B. Beaurepaire, F. Böhle, M. Bocoum, M. Lozano, A. Jullien, R. Lopez-Martens, A. Lifschitz, and J. Faure, Nat. Photonics **11**, 293 (2017).
[13] D. Gustas, D. Guénot, A. Vernier, S. Dutt, F. Böhle, R. Lopez-Martens, A. Lifschitz, and J. Faure, Phys. Rev. Accel. Beams **21**, 013401 (2018).
[14] J. Faure, D. Gustas, D. Guénot, A. Vernier, F. Böhle, M. Ouillé, S. Haessler, R. Lopez-Martens, and A. Lifschitz, Plasma Phys. Controlled Fusion **61**, 014012 (2019).
[15] Z.-H. He, A. G. R. Thomas, B. Beaurepaire, J. A. Nees, B. Hou, V. Malka, K. Krushelnick, and J. Faure, Appl. Phys. Lett. **102**, 064104 (2013).
[16] F. Salehi, M. Le, L. Railing, and H. M. Milchberg, arXiv:2010.15720 (2020).
[17] H. Fattahi, H. G. Barros, M. Gorjan, T. Nubbemeyer, B. Alsaif, C. Y. Teisset, M. Schultze, S. Prinz, M. Haefner, M. Ueffing, A. Alismail, L. Vámos, A. Schwarz, O. Pronin, J. Brons, X. T. Geng, G. Arisholm, M. Ciappina, V. S. Yakovlev, D.-E. Kim, A. M. Azzeer, N. Karpowicz, D. Sutter, Z. Major, T. Metzger, and F. Krausz, Optica **1**, 45 (2014).
[18] J. Henrich, S. Butcher, and M. Arrigoni, *Laser Focus World* (Endeavor Business Media, 2020), p. 1.
[19] Z.-H. He, B. Hou, J. A. Nees, J. H. Easter, J. Faure, K. Krushelnick, and A. G. R. Thomas, New J. Phys. **15**, 053016 (2013).
[20] F. Salehi, A. J. Goers, G. A. Hine, L. Feder, D. Kuk, B. Miao, D. Woodbury, K. Y. Kim, and H. M. Milchberg, Opt. Lett. **42**, 215 (2017).
[21] J. Krall, A. Ting, E. Esarey, and P. Sprangle, Phys. Rev. E **48**, 2157 (1993).
[22] D. L. Fisher and T. Tajima, Phys. Rev. E **53**, 1844 (1996).

[23]H. Ekerfelt, *Numerical and Experimental Studies of Wakefield Accelerators* (Lund University, 2019).
[24]S. Semushin and V. Malka, Rev. Sci. Instrum. **72**, 2961 (2001).
[25]J. L. Henares, P. Puyuelo-Valdes, F. Hannachi, T. Ceccotti, M. Ehret, F. Gobet, L. Lancia, J.-R. Marquès, J. J. Santos, M. Versteegen, and M. Tarisien, Rev. Sci. Instrum. **90**, 063302 (2019).
[26]F. Salehi, A. J. Goers, L. Feder, B. Miao, D. Woodbury, and H. M. Milchberg, Rev. Sci. Instrum. **90**, 103001 (2019).
[27]B. Hidding, K.-U. Amthor, B. Liesfeld, H. Schwoerer, S. Karsch, M. Geissler, L. Veisz, K. Schmid, J. G. Gallacher, S. P. Jamison, D. Jaroszynski, G. Pretzler, and R. Sauerbrey, Phys. Rev. Lett. **96**, 105004 (2006).
[28]M. Mori, M. Kando, I. Daito, H. Kotaki, Y. Hayashi, A. Yamazaki, K. Ogura, A. Sagisaka, J. Koga, K. Nakajima, H. Daido, S. V. Bulanov, and T. Kimura, Phys. Lett. A **356**, 146 (2006).
[29]B. Hidding, M. Geissler, G. Pretzler, K.-U. Amthor, H. Schwoerer, S. Karsch, L. Veisz, K. Schmid, and R. Sauerbrey, Phys. Plasmas **16**, 043105 (2009).
[30]S. Masuda and E. Miura, Phys. Plasmas **16**, 093105 (2009).
[31]S.-Y. Chen, M. Krishnan, A. Maksimchuk, R. Wagner, and D. Umstadter, Phys. Plasmas **6**, 4739 (1999).
[32]A. J. Goers, G. A. Hine, L. Feder, B. Miao, F. Salehi, J. K. Wahlstrand, and H. M. Milchberg, Phys. Rev. Lett. **115**, 194802 (2015).
[33]C.-Y. Hsieh, M.-W. Lin, and S.-H. Chen, Phys. Plasmas **25**, 023101 (2018).
[34]D. Woodbury, L. Feder, V. Shumakova, C. Gollner, R. Schwartz, B. Miao, F. Salehi, A. Korolov, A. Pugžlys, A. Baltuška, and H. M. Milchberg, Opt. Lett. **43**, 1131 (2018).
[35]S. V. Bulanov, M. Yamagiwa, T. Z. Esirkepov, D. V. Dylov, F. F. Kamenets, N. S. Knyazev, J. K. Koga, M. Kando, Y. Ueshima, K. Saito, and D. Wakabayashi, Plasma Phys. Rep. **32**, 263 (2006).
[36]S. Gordienko and A. Pukhov, Phys. Plasmas **12**, 043109 (2005).
[37]K. Nakajima, D. Fisher, T. Kawakubo, H. Nakanishi, A. Ogata, Y. Kato, Y. Kitagawa, R. Kodama, K. Mima, H. Shiraga, K. Suzuki, K. Yamakawa, T. Zhang, Y. Sakawa, T. Shoji, Y. Nishida, N. Yugami, M. Downer, and T. Tajima, Phys. Rev. Lett. **74**, 4428 (1995).
[38]E. Esarey, B. A. Shadwick, P. Catravas, and W. P. Leemans, Phys. Rev. E **65**, 056505 (2002).
[39]A. Pukhov, Z.-M. Sheng, and J. Meyer-ter-Vehn, Phys. Plasmas **6**, 2847 (1999).
[40]T. Wang, V. Khudik, A. Arefiev, and G. Shvets, Phys. Plasmas **26**, 083101 (2019).
[41]J. L. Shaw, N. Lemos, K. A. Marsh, D. H. Froula, and C. Joshi, Plasma Phys. Controlled Fusion **60**, 044012 (2018).
[42]C. B. Schroeder and E. Esarey, Phys. Rev. E **81**, 056403 (2010).
[43]J. L. Shaw, F. S. Tsung, N. Vafaei-Najafabadi, K. A. Marsh, N. Lemos, W. B. Mori, and C. Joshi, Plasma Phys. Controlled Fusion **56**, 084006 (2014).
[44]A. Pukhov, Rep. Prog. Phys. **66**, 47 (2003).
[45]N. Lemos, J. L. Martins, F. S. Tsung, J. L. Shaw, K. A. Marsh, F. Albert, B. B. Pollock, and C. Joshi, Plasma Phys. Controlled Fusion **58**, 034018 (2016).
[46]B. S. Nicks, T. Tajima, D. Roa, A. Nečas, and G. Mourou, Int. J. Mod. Phys. A **34**, 1943016 (2019).
[47]R. Lehe, M. Kirchen, I. A. Andriyash, B. B. Godfrey, and J.-L. Vay, Comput. Phys. Commun. **203**, 66 (2016).
[48]M. V. Ammosov, N. B. Delone, and V. P. Krainov, JETP **64**, 1191 (1986).
[49]J. L. Shaw, N. Lemos, K. A. Marsh, F. S. Tsung, W. B. Mori, and C. Joshi, Plasma Phys. Controlled Fusion **58**, 034008 (2016).
[50]FBPIC Contributors, FBPIC documentation, 2020.
[51]K. Schmid and L. Veisz, Rev. Sci. Instrum. **83**, 053304 (2012).
[52]J. P. Couperus, A. Köhler, T. A. W. Wolterink, A. Jochmann, O. Zarini, H. M. J. Bastiaens, K. J. Boller, A. Irman, and U. Schramm, Nucl. Instrum. Methods Phys. Res., Sect. A **830**, 504 (2016).
[53]M. C. Downer, R. Zgadzaj, A. Debus, U. Schramm, and M. C. Kaluza, Rev. Mod. Phys. **90**, 035002 (2018).
[54]N. Lemos, F. Albert, J. L. Shaw, D. Papp, R. Polanek, P. King, A. L. Milder, K. A. Marsh, A. Pak, B. B. Pollock, B. M. Hegelich, J. D. Moody, J. Park, R. Tommasini, G. J. Williams, H. Chen, and C. Joshi, Plasma Phys. Controlled Fusion **60**, 054008 (2018).
[55]M.-W. Lin, T.-Y. Chu, Y.-Z. Chen, D. K. Tran, H.-H. Chu, S.-H. Chen, and J. Wang, Phys. Plasmas **27**, 113102 (2020).
[56]W. Lu, C. Huang, M. Zhou, M. Tzoufras, F. S. Tsung, W. B. Mori, and T. Katsouleas, Phys. Plasmas **13**, 056709 (2006).
[57]W. Lu, M. Tzoufras, C. Joshi, F. S. Tsung, W. B. Mori, J. Vieira, R. A. Fonseca, and L. O. Silva, Phys. Rev. Spec. Top.–Accel. Beams **10**, 061301 (2007).
[58]B. Beaurepaire, A. Lifschitz, and J. Faure, New J. Phys. **16**, 023023 (2014).
[59]L. Rovige, J. Huijts, I. A. Andriyash, A. Vernier, M. Ouillé, Z. Cheng, T. Asai, Y. Fukuda, V. Tomkus, V. Girdauskas, G. Raciukaitis, J. Dudutis, V. Stankevic, P. Gecys, R. Lopez-Martens, and J. Faure, Phys. Plasmas **28**, 033105 (2021).
[60]L. Rovige, J. Huijts, I. Andriyash, A. Vernier, V. Tomkus, V. Girdauskas, G. Raciukaitis, J. Dudutis, V. Stankevic, P. Gecys, M. Ouille, Z. Cheng, R. Lopez-Martens, and J. Faure, Phys. Rev. Accel. Beams **23**, 093401 (2020).